Design and simulation of deep-well GaAs-based quantum cascade lasers for 6.7 μm room-temperature operation

X. Gao, M. D'Souza, D. Botez, and I. Knezevic[a)]
Department of Electrical and Computer Engineering, University of Wisconsin—Madison, 1415 Engineering Drive, Madison, Wisconsin 53706-1691, USA

(Received 8 September 2007; accepted 15 October 2007; published online 7 December 2007)

We present the design and simulation of a GaAs-based quantum cascade laser (QCL) emitting at 6.7 μm, the shortest room-temperature lasing wavelength projected to date for GaAs-based QCLs. This is achieved by introducing compressive strain only in the active quantum wells, where the optical transition occurs. A Monte Carlo simulation including both Γ- and *X*-valley transport demonstrates that the proposed QCL achieves room-temperature lasing at a threshold-current density of 14 kA/cm^2, lower than that of the conventional 9.4 μm QCL (16.7 kA/cm^2). Furthermore, the electron temperature at 300 K lattice temperature is similar to that of the 9.4 μm device. © *2007 American Institute of Physics*. [DOI: 10.1063/1.2820039]

I. INTRODUCTION

The $Al_{0.45}Ga_{0.55}As/GaAs$ quantum cascade laser (QCL) by Page *et al.*,[1] emitting at 9.4 μm, has shown the best device performance so far among GaAs-based mid-infrared quantum cascade lasers (QCLs). It can achieve pulsed room-temperature operation and operate in continuous mode up to 150 K.[2] The superior performance of this particular design is due to the relatively large (370 meV) Γ-point conduction band offset between the wells and barriers, which minimizes the leakage arising from the scattering of carriers from the injector states to the Γ-valley continuum states,[3] and also indirectly results in very small leakage to the *X*-valleys even at room temperature.[4,5]

To decrease the room-temperature emission wavelength of $Al_xGa_{1-x}As/GaAs$ QCLs below 9 μm, one alternative is to deposit InAs monolayers in the active quantum wells (QWs).[6] This way, Carder *et al.*[6] achieved room-temperature pulsed lasing at 8.5 μm. Wilson *et al.*[7] have shown that, in AlAs/GaAs QCLs incorporating a single injection barrier, once the upper lasing level becomes aligned with the lowest *X*-valley state of the injection barrier, lasing is suppressed due to intervalley (Γ-*X*) electron transfer, which limits the emission wavelengths to above 8 μm. Utilizing a double injection barrier,[7] however, reduced the emission wavelength to 7.3 μm, the shortest wavelength so far reported in GaAs-based QCLs, with pulsed lasing observed only at cryogenic temperatures.

In this paper, we present a design for GaAs-based QCL devices, which shows that, for a given lattice-matched QCL structure, one can significantly shorten the emission wavelength at *no* penalty in device performance by introducing compressive strain only in the active QWs, and tensile strain in a layer adjacent to the injection barrier. Specifically, by using a Monte Carlo simulator including both Γ- and *X*-valley transport,[4] we demonstrate that using $In_{0.1}Ga_{0.9}As$ active QWs in the 9.4 μm $Al_{0.45}Ga_{0.55}As/GaAs$ QCL structure of Page *et al.*, with modified layer thicknesses, provides room-temperature lasing at 6.7 μm with a slightly lower threshold-current density (14 kA/cm^2) than obtained for the 9.4 μm QCL (Ref. 1) (16.7 kA/cm^2). This approach to significantly shorten the wavelength is extendable to lattice-matched InP-based devices[8,9] for lowering their emission wavelength below 7 μm, and it is much simpler to implement and potentially more reliable than the current approach (i.e., compressively straining *all* QWs and tensilely straining *all* barriers[10,11]).

II. THE DEEP-WELL STRUCTURE

The concept of utilizing deep wells in the active region (strained $In_xGa_{1-x}As$ active wells in GaAs-based devices) in order to significantly shorten the emission wavelength was demonstrated on single-stage $In_{0.3}Ga_{0.7}As/Al_{0.7}Ga_{0.3}As/GaAs$ devices, which provided strong electroluminescence at 4.7 μm (Ref. 12) and were not strain compensated. A similar concept was applied to the not-strain-compensated, deep-well $In_{0.4}Ga_{0.96}As/Al_{0.33}Ga_{0.67}As/GaAs$ devices,[13] emitting at 10.4 and 9.45 μm up to a maximum temperature of 200 K. Our proposed laser structure employs the conventional three-well active region design,[1] but utilizes strained $In_{0.1}Ga_{0.9}As$ in the two wide active QWs to achieve a room-temperature emission wavelength below 7 μm, with the strain compensated within each stage. The calculated conduction band profile and the moduli squared of the relevant Γ- and *X*-valley wave functions in two adjacent stages for the proposed QCL are depicted in Fig. 1, where the Γ-states are solved for using the $\mathbf{k}\cdot\mathbf{p}$ method and the *X*-states are obtained within the effective mass framework.[4,14] To partially compensate the compressive strain in the $In_{0.1}Ga_{0.9}As$ layers, one $GaAs_{0.6}P_{0.4}$ layer is added just to the left of the injection barrier. The resulting net compressive strain within one stage is 0.07 %, calculated using the model-solid theory.[15]

The Γ-point conduction band offset between the strained $In_{0.1}Ga_{0.9}As$ well and the $Al_{0.45}Ga_{0.55}As$ barrier (the strain-induced offset is included using the model-solid theory[15]) is 45 meV larger than that between the GaAs well and the $Al_{0.45}Ga_{0.55}As$ barrier. The radiative transition energy (3

[a)]Electronic mail: knezevic@engr.wisc.edu.

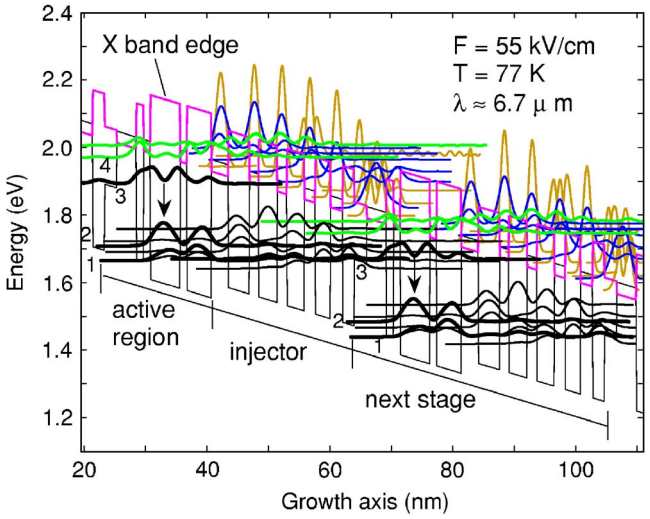

FIG. 1. (Color online) Conduction band profile and the moduli squared of the relevant Γ- and *X*- wave functions in two adjacent stages of the proposed $In_{0.1}Ga_{0.9}As/Al_{0.45}Ga_{0.55}As/GaAs$ laser design. The bold black lines denote the active lasing levels (3: upper, 2: lower, 1: ground). The thin black lines are the injector miniband states, and the bold green lines are the Γ continuum states (Γ_c). Level 4 denotes the first Γ_c-state. The thin blue lines denote the doubly degenerate X_x states, and the yellow lines are the X_z states. The arrow denotes the lasing transition. The layer sequence of one stage (in Å) starting from the $GaAs_{0.6}P_{0.4}$ barrier layer on the left is ***20***, **32**, 12, **11**, {48}, **11**, {40}, **28**, 34, **15**, 30, **16**, 28, **18**, 25, **20**, 19. The bold italic script denotes the $GaAs_{0.6}P_{0.4}$ barrier, the bold script the $Al_{0.45}Ga_{0.55}As$ barriers, the normal script the GaAs wells, and the values in curly brackets indicate the $In_{0.1}Ga_{0.9}As$ wells. The underlined layers are *n*-type doped with a sheet doping density of $N_s=3.8\times10^{11}$ cm^{-2}. The calculated energy difference is $E_{32}=185$ meV ($\lambda\approx6.7$ μm).

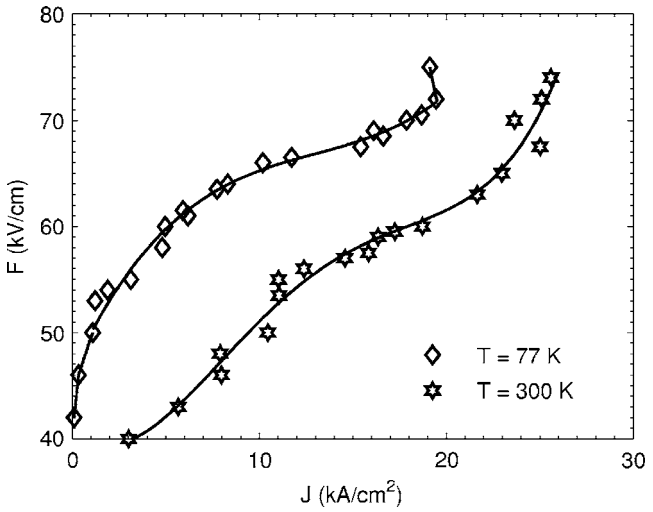

FIG. 2. Electric field vs current density for the proposed QCL structure at the lattice temperatures of 77 K and 300 K. The solid lines are polynomial fits to the data points.

$\rightarrow$2) is 185 meV, about 54 meV larger than 131 meV for the 9.4 μm 45% Al QCL. While the upper lasing level of the proposed structure is 20 meV closer to the Γ-band edge due to the thinner active region wells, the remaining 34 meV increase in the transition energy is thanks to the deep wells in the active region. The thinner active region wells also enable the lowest Γ-continuum level (level 4 in Fig. 1) to shift up by 15 meV, which helps to reduce leakage to the continuum.[4] The calculated lifetime due to the electron-longitudinal optical (electron-LO) phonon interaction for level 3 is $\tau_3=1.5$ ps, where $1/\tau_3=1/\tau_{32}+1/\tau_{31}$, $\tau_{32}=2.5$ ps, and $\tau_{31}=3.8$ ps. The lifetime of level 2 is $\tau_2\approx\tau_{21}=0.3$ ps. The dipole matrix element $\langle z_{32}\rangle$ is calculated to be 1.5 nm. These calculations were done at $F=55$ kV/cm, close to the estimated threshold field of $F=58$ kV/cm (see Figs. 2 and 3) and $T=77$ K. The lifetimes and matrix element are similar to those of the 9.4 μm 45% Al QCL ($\tau_3=1.4$ ps, $\tau_2=0.3$ ps, and $\langle z_{32}\rangle=1.7$ nm).[1]

III. SIMULATED PERFORMANCE CHARACTERISTICS

To simulate the output characteristics of the proposed QCL structure, we employ a Monte Carlo simulator[4,14] that takes into account both Γ- and *X*-valley transport and includes all the relevant scattering mechanisms: electron-LO phonon, electron-electron, and intervalley scattering processes within the same stage and between adjacent stages. The Monte Carlo simulation yields the current density *J*, the electron density in each subband, and the electron temperature T_e for a given electric field. The modal gain G_m can then be calculated from the population inversion (i.e., the electron density difference between the upper and lower lasing levels) and the waveguide confinement factor Γ_w. Based on the estimate of the waveguide losses α_w and mirror losses α_m, a realistic threshold-current density can be determined.

A. Modal gain. Threshold current density

The modal gain G_m is proportional to the population inversion Δn and is given under the steady-state conditions by[16]

$$G_m=\frac{4\pi e^2}{\varepsilon_0 \underline{n}}\frac{\langle z_{32}\rangle^2}{2\gamma_{32}L_p\lambda}\Gamma_w\Delta n=g\Gamma_w J, \tag{1}$$

where ε_0 is the vacuum dielectric permittivity, $\underline{n}$ is the optical mode refractive index, $2\gamma_{32}$ is the full width at half maximum of the electroluminescence spectrum below threshold, L_p is the length of one stage, λ is the laser emission wavelength, $\langle z_{32}\rangle$ is the dipole matrix element, and Γ_w is the waveguide confinement factor. The waveguide is designed such that the 25-stage active region is sandwiched between two 1.3 μm thick, low-doped (4×10^{16} cm^{-3}) GaAs layers. (Only 25 stages are expected to be grown considering that the residual strain may cause dislocations in the crystal lattice.) The GaAs layers are followed by 0.3 μm thick $Al_{0.9}Ga_{0.1}As$ cladding layers (doped to 1×10^{18} cm^{-3}) and 1 μm thick GaAs layers (doped to 4×10^{16} cm^{-3}). On one side of the above layer sequence is a 1 μm thick, highly doped (5×10^{18} cm^{-3}) GaAs contact layer, and on the other side is a 1 μm thick, highly doped (5×10^{18} cm^{-3}) GaAs cladding layer and the GaAs substrate. The parameters of the designed waveguide are calculated to be $\Gamma_w=33\%$, $\underline{n}=3.21$, and $\alpha_w=15$ cm^{-1}. Even with fewer stages, the addition of $Al_{0.9}Ga_{0.1}As$ cladding layers allows for a Γ_w value higher than 28%, the value used in the 36-stage 9.4 μm 45% Al QCL.[1] The calculated waveguide losses are lower than those of the 9.4 μm 45% Al QCL (20 cm^{-1}), due to a reduction in the free-carrier absorption with decreasing wavelength.[17] L_p

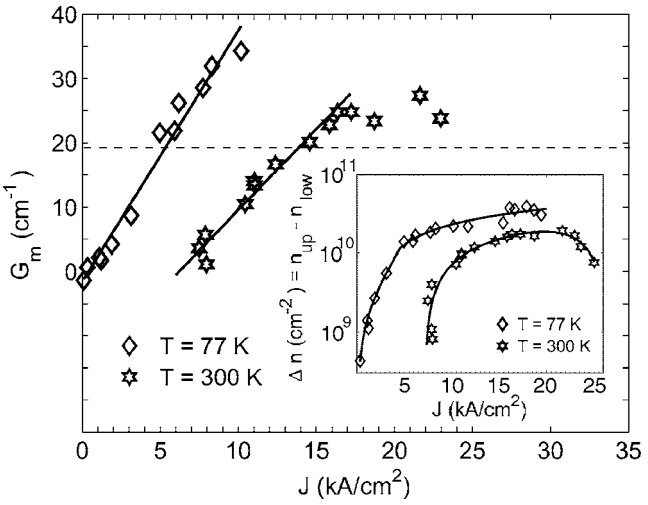

FIG. 3. Modal gain vs current density at the lattice temperatures of 77 K and 300 K. The horizontal dashed line indicates the calculated total losses $\alpha_w + \alpha_m = 19$ cm^{-1}. The solid lines are linear fits to the data points in the region of relatively low current density, whose intercept with the loss line gives the threshold current density J_{th}. Inset: Population inversion vs current density at 77 K and 300 K.

$=40.7$ nm, while $2\gamma_{32}=12$ meV at 77 K and 22 meV at 300 K (values taken from Ref. 1).

Figure 2 shows the calculated electric field versus current density characteristics of the proposed QCL structure at the lattice temperatures of 77 K and 300 K. The computed current density values include the leakage currents through the next-stage Γ-continuum states and the *X*-valley states.[14] The saturation currents (20 kA/cm^2 at 77 K and 25 kA/cm^2 at 300 K) are comparable to the values for the 9.4 μm 45% Al QCL.[1] Given the waveguide parameters, the G_m versus J relation obtained is shown in Fig. 3. Following Eq. (1), the gain coefficient g is obtained as $g=11.8$ cm/kA ($T=77$ K) and $g=7.6$ cm/kA ($T=300$ K) for the proposed laser, which are similar to the calculations by Indjin *et al.*[18] for the 9.4 μm 45% Al QCL ($g=11$ cm/kA at 77 K and $g=5$ cm/kA at 300 K). Given the calculated total losses $\alpha_m + \alpha_w = 19$ cm^{-1} ($\alpha_m = 4$ cm^{-1}), the threshold-current density J_{th} is found to be 5 kA/cm^2 at 77 K and 14 kA/cm^2 at 300 K (Fig. 3).[19] [For comparison, J_{th} at 300 K for the 9.4 μm QCL (Ref. 1) is 16.7 kA/cm^2.] At 300 K, the modal gain of the proposed structure saturates in the high-J range (above 17 kA/cm^2) due to the carrier loss to the *X*-valleys[14] that results in reduced population inversion (inset of Fig. 3). Nevertheless, the saturation gain (~25 cm^{-1}) is sufficiently high with respect to the total losses of 19 cm^{-1} to deem room-temperature operation of the proposed QCL quite feasible.

B. *X*-valley leakage

With the shortening of the wavelength, enhanced leakage to the Γ-continuum (Γ_c) states and the *X*-valley states becomes a concern. In our recent work,[4,14] we have shown that the dominant *X*-valley leakage path in GaAs-based QCLs is interstage $X \rightarrow X$ scattering, a result of the following three-stage process: (1) In the case of appreciable overlap between the Γ-localized (Γ_l) states in one stage and Γ_c states in the next stage, leakage to Γ_c occurs. (2) A portion of the electrons that have leaked into Γ_c do not remain there, but rather end up in the same-stage *X*-valley states. $\Gamma_c \rightarrow X$ same-stage scattering is very efficient (provided there are enough intervalley phonons to enable the transition) due to these wave functions' large overlap and the high effective mass of the *X*-valley subbands. The inverse scattering is significantly less efficient, because of the Γ-valley lower mass, so carriers once scattered into *X* tend to remain in *X* rather than go back to Γ. (3) With enough population in the *X*-valley subbands, $X \rightarrow X$ scattering between adjacent stages occurs, because the *X*-valley subbands are generally poorly confined so the overlap among the subbands in neighboring stages is appreciable. Therefore, significant overlap between Γ_l and the next stage Γ_c states causes not only the leakage to continuum, but also significant $X \rightarrow X$ leakage.[4,14]

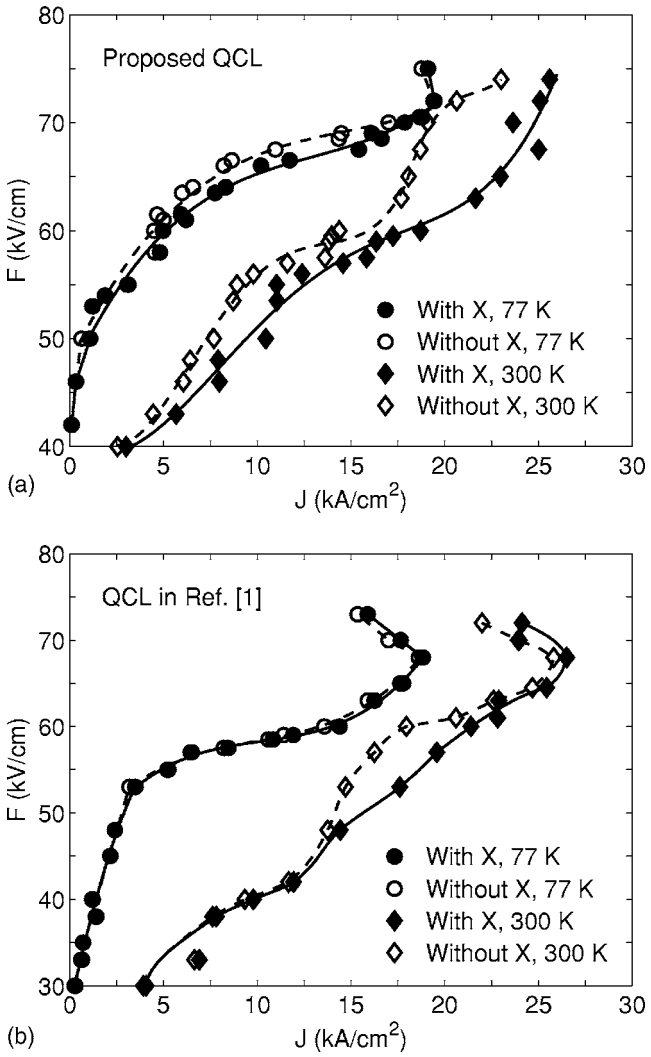

FIG. 4. Electric field vs current density for the proposed QCL structure (a) and the 9.4 μm QCL from Ref. 1 (b) at the lattice temperatures of 77 and 300 K, with and without the inclusion of the *X*-valley transport in the simulation. The lines are polynomial fits to the data points.

In Fig. 4, electric field versus current density for the proposed QCL (a) and the 9.4 μm QCL of Ref. 1 (b) are presented, at 77 K and 300 K lattice temperatures, with and without the *X*-valley leakage. At both 77 K and 300 K, the *X*-valley leakage current in the proposed QCL is higher than in the 9.4 μm QCL of Page *et al.* (At 77 K, the leakage in

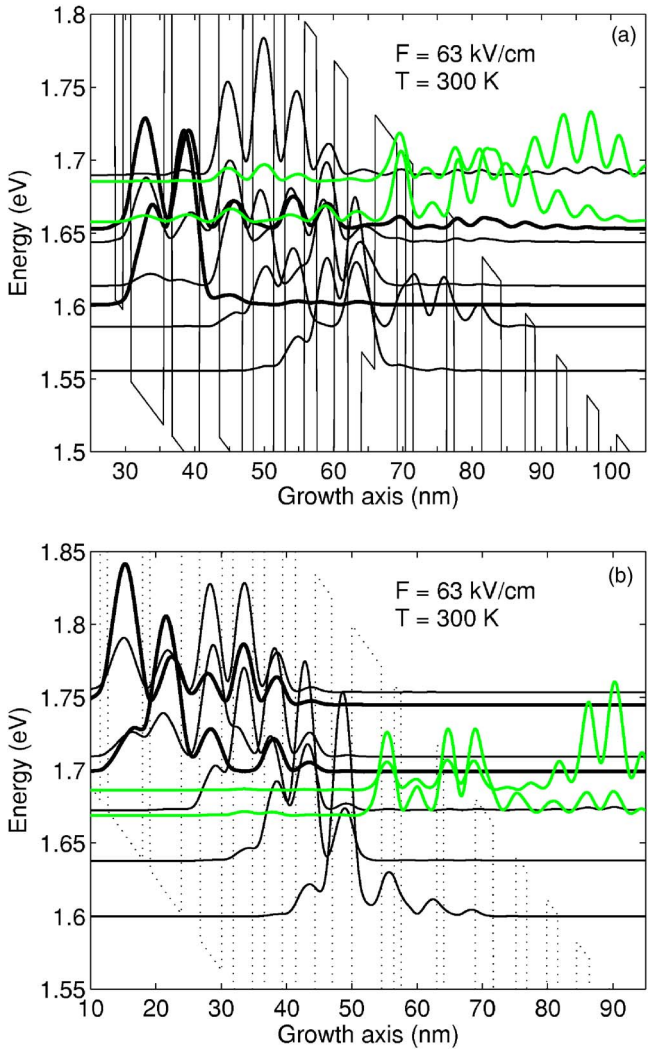

FIG. 5. (Color online) Blow-up of the wave function moduli squared of the injector miniband and the next-stage Γ-continuum states in the proposed QCL (a) and the 9.4 μm structure of Page *et al.*[1] (b), at the field of 63 kA/cm (above threshold for both structures). Black lines denote the injector states (bold black lines are the lower lasing level 2 and the ground state 1), while the green lines denote the next-stage Γ-continuum states. Significant overlap between the injector miniband states and the Γ-continuum states results not only in direct carrier loss to the Γ-continuum states, but indirectly in high current through the *X*-valley states, through the mechanism described in Ref. 4. The overlap is greater in the proposed structure (a) than the QCL of Ref. 1 (b).

both structures is fairly low, predominantly due to a low number of intervalley phonons.) As seen in Fig. 5, the reason is the difference in the overlap between the injector miniband and the next-stage continuum states: the structure of Page *et al.* has a remarkably low overlap [Fig. 5(b)] between the miniband and the next-stage Γ_c; in the proposed structure, however, this overlap is greater [Fig. 5(a)], which results in a somewhat higher *X*-valley leakage current for a given electric field. However, even with more *X*-valley leakage, the total current at a given field is significantly lower in the proposed structure than in the 9.4 μm QCL of Page *et al.*, owing to the design modification necessary for the wavelength shortening.

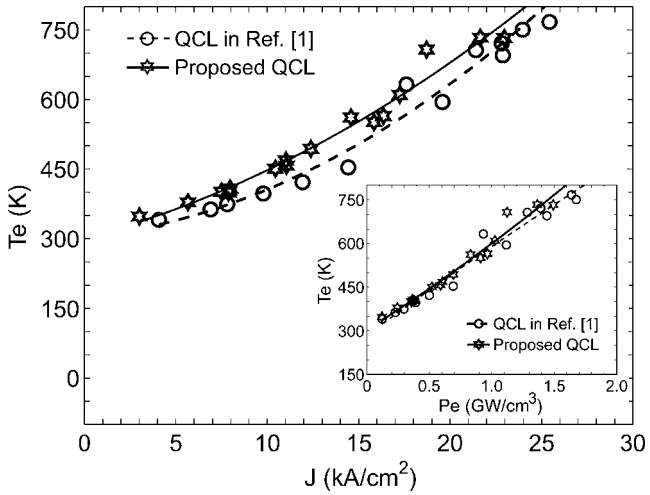

FIG. 6. Electron temperature T_e vs current density J for the proposed 6.7 μm QCL and the 9.4 μm QCL structure of Page *et al.*,[1] at the lattice temperature of 300 K. The lines are polynomial fits, intended to guide the eye. Inset: Electron temperature vs input electrical power density $P_e=JF$ for the two structures.

C. Electron heating

The electron temperature T_e, generally higher than the lattice temperature, characterizes the degree of electron heating in a QCL device. With relatively high carrier densities per subband, the distribution function within each subband *i* becomes Maxwellian $[f(E_{k,i}) \sim \exp(-E_{k,i}/k_B T_e)]$ as a result of efficient carrier-carrier intra-subband scattering (intersubband scattering, both electron-electron and electron-phonon, is less efficient). The electronic temperature T_e is approximately the same for all subbands.[20,21] In the Monte Carlo simulation, the electron temperature can be obtained either from the thermalized distribution function above or from the ensemble average of the carrier kinetic energy $T_e = \langle E_k \rangle / k_B$ (these two approaches are equivalent as long as the distribution is Maxwellian), and in this work we use the latter approach.

Figure 6 shows the electron temperature as a function of the current density J for the proposed 6.7 μm structure and the 9.4 μm QCL,[1] as well as a function of the input power density (inset), at the lattice temperature of 300 K. It is clear that the reduction in the room-temperature emission wavelength, provided by the proposed deep-well structure, is achieved at no penalty in the electron heating: at threshold, the electron temperatures are $T_e=530$ K ($J_{\text{th}}=14$ kA/cm^2) for the proposed structure and $T_e=544$ K ($J_{\text{th}}=16.7$ kA/cm^2) for the 9.4 μm QCL of Page *et al.*[1] (We find very little influence of the *X*-valley transport on the electron temperature, up to very high electric fields, and therefore do not separate the curves with and without *X*-valley transport. The reason is low *X*-valley population and generally low kinetic energy in these subbands, up to high electric fields.[22])

In both structures, the variation of the electronic temperature with the current density is linear only for very low current densities (Fig. 6), with the low-current electron-lattice coupling constant being $\lim_{J\to 0}[(T_e - T_L)/J] \approx 14$ K cm^2/kA for both structures. However, the variation

of T_e with the power density (JF) obeys a linear law up to high power densities (inset of Fig. 6). This agrees with a simple energy-balance equation,

$$nk_B\frac{d(T_e-T_L)}{dt}=JF-nk_B\frac{(T_e-T_L)}{\tau_E}, \tag{2}$$

where n is the total carrier density and τ_E is an effective (ensemble averaged) energy relaxation time.[23] In the steady state, the above equation yields

$$T_e-T_L=\frac{\tau_E}{nk_B}JF, \tag{3}$$

which is a simple, intuitive description of the linear behavior that we observe in the simulation (inset of Fig. 6).

For the structure of Page *et al.*, the University of Bari group recently reported[24] a projected electronic temperature of about 800 K at threshold, with the heatsink temperature of 243 K and an estimated lattice temperature of 300 K. The temperature they reported is about 250 K higher than what we obtain for the same lattice temperature and at threshold (Fig. 6). There are several reasons for the discrepancy. First, we perform all the simulations at a given lattice temperature, rather than at a given heatsink temperature, because a specified lattice temperature is necessary for the calculation of the scattering rates that enter our simulator. Therefore, we do not account for the thermal resistance,[25–27] which is a nontrivial thing to model in superlattices and certainly beyond the scope of this paper. Accounting for confined bulklike and interface phonons, as well as for the nonequilibrium phonon distribution at high fields, is important for the computation of the thermal resistance, but would also alter the scattering rates and further change the output of the electronic-transport simulation. Second, our calculation accounts for the transport through the laser's active region alone, and thus no effect of the actual waveguide is incorporated in the simulation. Therefore, it is not trivial to perform a direct comparison of our simulation results with the experimental data of Spagnolo *et al.*[24]

IV. SUMMARY

We have reported the design and simulation of a strain-compensated $In_{0.1}Ga_{0.9}As/Al_{0.45}Ga_{0.55}As/GaAs$ QCL emitting at 6.7 μm, using a Monte Carlo simulator that includes both Γ- and X-valley transport. The designed QCL is predicted to yield sufficient gain for lasing action up to at least 300 K, in conjunction with the proposed waveguide design. The threshold current density is estimated to be 5 kA/cm^2 at 77 K and 14 kA/cm^2 at 300 K. Electron heating at room temperature is similar to that of the 9.4 μm $Al_{0.45}Ga_{0.55}As/GaAs$ QCL. Therefore, the use of deep active quantum wells appears to be an attractive design approach for high performance GaAs-based QCLs at wavelengths below 7 μm, as well as for shortening the wavelength of InP-based QCLs.

ACKNOWLEDGMENTS

The authors X.G. and M.D.S. made qualitatively equal contributions to this work.

[1] H. Page, C. Becker, A. Robertson, G. Glastre, V. Ortiz, and C. Sirtori, Appl. Phys. Lett. **78**, 3529 (2001).
[2] H. Page, S. Dhillon, M. Calligaro, C. Becker, V. Ortiz, and C. Sirtori, IEEE J. Quantum Electron. **40**, 665 (2004).
[3] C. Sirtori, H. Page, C. Becker, and V. Ortiz, IEEE J. Quantum Electron. **38**, 547 (2002).
[4] X. Gao, D. Botez, and I. Knezevic, Appl. Phys. Lett. **89**, 191119 (2006).
[5] S. R. Jin, C. N. Ahmad, S. J. Sweeney, A. R. Adams, B. N. Murdin, H. Page, X. Marcadet, C. Sirtori, and S. Tomic, Appl. Phys. Lett. **89**, 221105 (2006).
[6] D. A. Carder, L. R. Wilson, R. P. Green, J. W. Cockburn, M. Hopkinson, M. J. Steer, R. Airey, and G. Hill, Appl. Phys. Lett. **82**, 3409 (2003).
[7] L. R. Wilson, D. A. Carde, J. W. Cockburn, R. P. Green, D. G. Revin, M. J. Steer, M. Hopkinson, G. Hill, and R. Airey, Appl. Phys. Lett. **81**, 1378 (2002).
[8] M. Troccoli, D. Bour, S. Corzine, G. Höfler, A. Tandon, D. Mars, D. J. Smith, L. Diehl, and F. Capasso, Appl. Phys. Lett. **85**, 5842 (2004).
[9] Z. Liu, D. Wasserman, S. S. Howard, A. J. Hoffman, C. F. Gmachl, X. Wang, T. Tanbun-Ek, L. Cheng, and F.-S. Choa, IEEE Photon. Technol. Lett. **18**, 1347 (2006).
[10] A. Evans, J. S. Yu, J. David, L. Doris, K. Mi, S. Slivken, and M. Razeghi, Appl. Phys. Lett. **84**, 314 (2004).
[11] S. Blaser, D. A. Yarekha, L. Hvozdara, Y. Bonetti, A. Muller, M. Giovannini, and J. Faist, Appl. Phys. Lett. **86**, 041109 (2005).
[12] D. P. Xu, A. Mirabedini, M. D'Souza, S. Li, D. Botez, A. Lyakh, Y. J. Shen, P. Zory, and C. Gmachl, Appl. Phys. Lett. **85**, 4573 (2004).
[13] S. Gianordoli, W. Schrenk, L. Hvozdara, N. Finger, G. Strasser, and E. Gornik, Appl. Phys. Lett. **76**, 3361 (2000).
[14] X. Gao, D. Botez, and I. Knezevic, J. Appl. Phys. **101**, 063101 (2007).
[15] C. G. Van de Walle, Phys. Rev. B **39**, 1871 (1989).
[16] A. Mirčetić, D. Indjin, Z. Ikonić, P. Harrison, V. Milanović, and R. W. Kelsall, J. Appl. Phys. **97**, 084506 (2005).
[17] W. G. Spitzer and J. M. Whelan, Phys. Rev. **114**, 59 (1959).
[18] D. Indjin, P. Harrison, R. W. Kelsall, and Z. Ikonić, Appl. Phys. Lett. **81**, 400 (2002).
[19] For a slightly different design, J_{th} is found to be as low as 9.5 kA/cm^2 at 300 K, but no lasing occurs at 77 K.
[20] R. C. Iotti and F. Rossi, Appl. Phys. Lett. **78**, 2902 (2001).
[21] P. Harrison, Appl. Phys. Lett. **75**, 2800 (1999).
[22] X. Gao, Ph.D. thesis, University of Wisconsin—Madison (2008).
[23] M. Lundstrom, *Fundamentals of Carrier Transport* (Cambridge U. P., Cambridge, 2000).
[24] V. Spagnolo, G. Scamarcio, H. Page, and C. Sirtori, Appl. Phys. Lett. **84**, 3690 (2004).
[25] M. Beck, D. Hofstetter, T. Aellen, J. Faist, U. Oesterle, M. Ilegems, E. Gini, and H. Melchior, Science **295**, 301 (2002).
[26] C. Pflügl, W. Schrenk, S. Anders, G. Strasser, C. Becker, C. Sirtori, Y. Bonetti, and A. Muller, Appl. Phys. Lett. **83**, 4698 (2003).
[27] J. S. Yu, S. Slivken, A. Evans, L. Doris, and M. Razeghi, Appl. Phys. Lett. **83**, 2503 (2003).